PCCP

RSC Publishing

PAPER

View Article Online
View Journal | View Issue

Cite this: *Phys. Chem. Chem. Phys.*, 2013, **15**, 19741

Relative contributions of quantum and double layer capacitance to the supercapacitor performance of carbon nanotubes in an ionic liquid

Alexander J. Pak,† Eunsu Paek† and Gyeong S. Hwang*

Received 21st June 2013,
Accepted 4th October 2013

DOI: 10.1039/c3cp52590b

www.rsc.org/pccp

Motivated by promising demonstrations of carbon nanotube (CNT) electrodes in supercapacitors, we evaluate the capacitive performance of a (6,6) CNT in [BMIM][PF_6] ionic liquid (IL), with particular attention to the relative contributions of the electric double layer (EDL) capacitance (C_D) at the CNT/IL interface and the quantum capacitance (C_Q) of the CNT. Our classical molecular dynamics simulations reveal that the use of the CNT improves C_D when compared to planar graphene, which we discuss in terms of how the electrode curvature affects both the electric field strength and IL packing density. In addition, according to density functional theory calculations, the C_Q of the CNT is constant and significantly larger than that of graphene near the Fermi level, which is a consequence of the larger number of available electron states in the CNT. Our study also shows that the relative performance of the CNT- and graphene-based electrodes can be a strong function of applied voltage, which we attribute to the shifting contributions of C_Q and C_D.

1. Introduction

Electrical double-layer capacitors (EDLCs), or supercapacitors, have become an increasingly important part of our energy storage landscape, primarily due to their advantageous power densities and lifetimes.[1,2] Room-temperature ionic liquids[3,4] (RTILs), ''solvent-free'' ions that are in the liquid state at room temperature, have attracted much interest as an electrolyte due to their wide electrochemical windows, high chemical and thermal stability, extremely low volatility, and nonflammability.[5,6] In addition, carbon-based materials (such as activated carbon and graphene) have shown considerable potential as supercapacitor electrodes due to their high specific surface area and good electrical conductivity.[1,5–9] EDLCs, however, have poor energy density when compared to batteries, which has motivated research into improving the capacitance of these devices.[9–17]

Recently, carbon nanotube (CNT)-based electrodes in EDLCs have demonstrated superior performance compared to conventional activated carbon electrodes.[18–23] In the case of vertically aligned arrays of multiwalled CNTs (MWCNTs), Honda and coworkers demonstrated that the capacitance was inversely related to the MWCNT diameter while directly proportional to the MWCNT packing density.[20] The origins of this behavior, however, are still poorly understood largely due to limited molecular-level characterization of the electrode–electrolyte interface. A few theoretical simulations have attempted to address how CNTs influence capacitance. Yang and coworkers simulated CNT forests in [TEA][BF_4] IL using molecular dynamics (MD) simulations; they demonstrated that the EDL capacitance (C_D) was enhanced as a result of increased CNT packing density.[24] The exohedral electric double-cylinder capacitor model, developed by Huang and coworkers and based on a classical geometric capacitor, suggested that C_D increased with decreasing CNT radius.[25] From MD simulations, Feng and coworkers also showed that a (5,5) CNT electrode resulted in at least a 30% enhancement in capacitance compared to planar graphene electrodes with 1-butyl-3-methyl-imidazolium hexafluorophosphate ([BMIM][PF_6]) and [BMIM][Cl] ILs.[26]

Studies to date, however, have been limited to the impact of electrode curvature on the EDL. But recent experimental[27,28] and theoretical[29,30] results have indicated that the total interfacial capacitance (C_T) of low-dimensional carbon electrodes, specifically graphene, strongly depends on the relative contributions of C_D and the electrode quantum capacitance (C_Q). Similarly, the C_Q of CNT-based electrodes may also influence the C_T. Yet, the relative roles of both C_Q and C_D in CNT-based EDLCs have yet to be reported.

In this paper, we investigate the interfacial capacitance, particularly the effect of CNT curvature, of metallic (6,6) CNT electrodes in [BMIM][PF_6] IL using combined density functional theory (DFT) and classical MD simulations. Our particular interest

Department of Chemical Engineering, The University of Texas at Austin, Texas 78712, USA. E-mail: gshwang@che.utexas.edu; Fax: +1 512 471 7060; Tel: +1 512 471 4847

† These authors equally contributed to this work.

lies in understanding the relative contributions of C_D and C_Q as compared to pristine graphene electrodes. First, we investigate the microstructure of [BMIM][PF_6] near the CNT electrode by varying the electrode excess surface charge using MD simulations, and use the calculated IL distribution to evaluate the potential variation and EDL integral capacitance. Then, we employ DFT calculations to estimate the C_Q of the (6,6) CNT. Based on the calculation results, we discuss the impact of electrode curvature on the capacitive performance, especially the curvature effect on C_Q and C_D in terms of applied voltage.

2. Methods

2.1. Classical molecular dynamics

We employed MD simulations with the OPLS-AA force field[31,32] to determine the microstructure of [BMIM][PF_6] near the CNT and graphene electrodes; details of the force field parameters can be found in ref. 29. As illustrated in Fig. 1, the CNT–IL system consists of 1095 [BMIM][PF_6] pairs surrounding a centered (6,6) CNT with a radius of 4.08 Å and 16 unit cells (384 C atoms) in a simulation domain that is 100 × 100 × 39.46 $Å^3$ with periodic boundary conditions in all three directions. The domain is large enough such that the electrolyte can maintain a bulk density of 1.33 g cm^{-3} at the radial edges of the system. For $\sigma = \pm 6.33$ and ± 0.40 μC cm^{-2}, the C atoms of each CNT were assigned uniform atomic charges; the corresponding number of coions were removed from the domain to maintain charge neutrality. The graphene–IL system consists of 346 [BMIM][PF_6] pairs between two graphene electrodes (34.18 × 34.53 $Å^2$) separated by 100 Å. For $\sigma = \pm 6.33$ and ± 0.40 μC cm^{-2}, the C atoms in graphene were also assigned uniform atomic charges. Additional details for the graphene case may be found in ref. 29.

We annealed and quenched each MD simulation initially at 1000 K for 0.5 ns followed by 0.5 ns at 300 K for two cycles, and then further equilibrated for 3 ns at 300 K using a timestep of 1 fs. Production runs were carried out for 4 ns with atomic positions recorded every 5 ps. All runs were in the NVT ensemble with the temperature controlled using a Nose–Hoover thermostat[33] with a 100 fs damping parameter. All MD simulations were performed using the Large-scale Atomic/Molecular Massively Parallel Simulator (LAMMPS) program.[34] MD results reported herein were obtained from the average of six independent simulations with different initial atomic configurations.

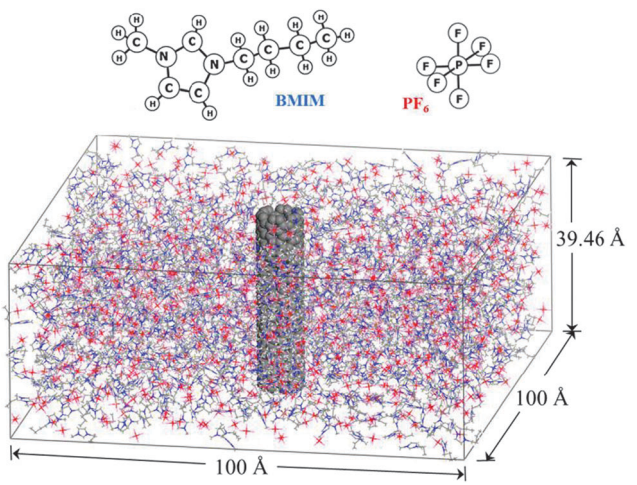

Fig. 1 Schematic of the CNT/IL simulation box; white, blue, and gray sticks indicate H, N, and C atoms in BMIM, and red and pink sticks indicate P and F atoms in PF_6. An infinite (*z* direction) (6,6) CNT is placed at the center of the domain, which is periodic in all three directions. The atomic structures of BMIM and PF_6 are also shown.

2.2. Density functional theory

The atomic and electronic structures of pristine graphene and (6,6) CNTs were calculated using DFT within the Perdew–Wang 91 generalized gradient approximation[35] (GGA-PW91), as implemented in the Vienna Ab initio Simulation Package[36] (VASP). We employed the projector augmented wave (PAW) method[37] to describe the interaction between core and valence electrons, and a planewave basis set with a kinetic energy cutoff of 400 eV. The CNT structure was modeled using periodic boundary conditions in all three directions; the supercell contained a (6,6) CNT with 5 unit cells corresponding to 12.33 Å in length and a vacuum space of 11.84 Å to avoid interactions with the periodic image. For the Brillouin zone integration, we used a (1 × 1 × 12) Monkhorst–Pack[38] *k*-point mesh for geometry optimization and energy calculations and a (1 × 1 × 32) Monkhorst–Pack *k*-point mesh for electronic structure calculations. Details of the calculations for pristine graphene can be found in ref. 29.

3. Results and discussion

3.1. Electric double layer microstructure and capacitance

The integral EDL capacitance can be obtained from the relationship between excess surface charge density (σ) and potential drop within the EDL (ϕ_D); that is, $C_D = \sigma/(\phi_D - \phi_Z)$, where ϕ_Z is known as the potential of zero charge (PZC). To obtain C_D, we first evaluated the [BMIM][PF_6] IL microstructure near the (6,6) CNT surface using MD simulations, as described in the following section.

Fig. 2 shows the mass density (ρ_m) profiles of cationic BMIM and anionic PF_6 at σ = 0.0 and ± 6.33 μC cm^{-2} near the CNT [(a)–(c)] and the pristine graphene [(d)–(f)] electrodes. Each panel displays some cation/anion layering as indicated by the oscillatory profiles. This layering tends to extend 2–3 nm from the electrode surface after which the IL structure becomes nearly bulk-like, which is consistent with previous molecular dynamics studies near planar[39–41] and cylindrical[26] surfaces. Note that experimental observations have demonstrated that the layers alternate between counter and co-ions near charged electrodes,[42,43] which is similarly seen here. In addition, it is possible to extrapolate insights on the orientation of electrolyte ions near both electrode surfaces, which we find to be in good agreement with past reports.[26,39–41] Near the positive electrodes [(b) and (e)], PF_6 exhibits three peaks which correspond to F, P, and F atoms, respectively; the electrostatic attraction between

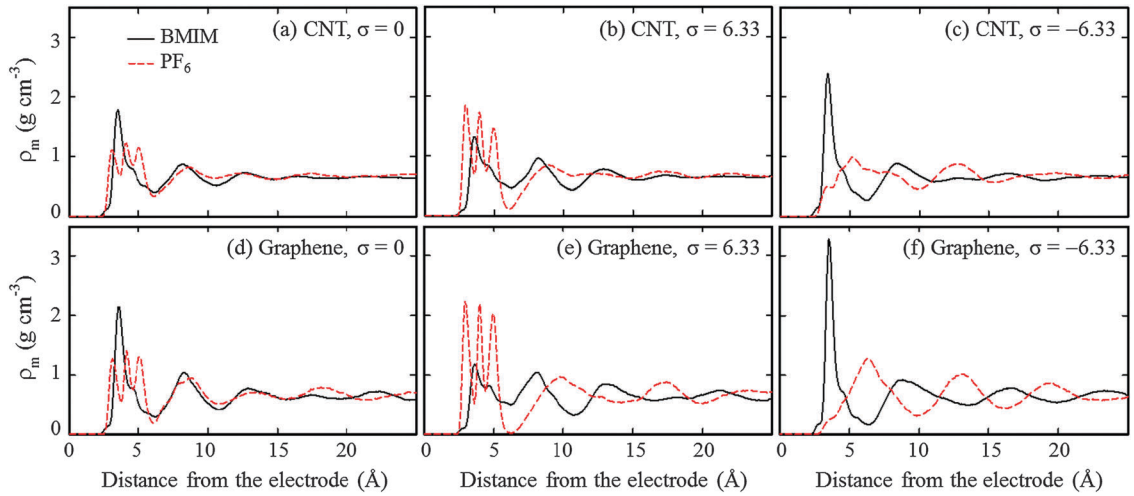

Fig. 2 Mass density (ρ_m) profiles of BMIM and PF_6 near (6,6) CNT [(a)–(c)] and pristine graphene [(d)–(f)] electrodes at the listed σ (in μC cm^{-2}) as a function of distance from the electrode surface.

the positive electrode and the negatively charged F atoms causes these planes of F atoms to orient parallel (concentric) to the graphene (CNT) surface. Similarly, the BMIM peak near the negative electrode [(c) and (f)] is comprised of atoms in the positively charged BMIM ring (not shown), which indicates the tendency of the ring to align parallel (concentric) to the graphene (CNT) surface. Note, however, that the plane of F atoms and the BMIM rings remain stiff and planar and do not actually conform to the CNT curvature.

In the case of the CNT electrodes, the mass density peaks appear to be diminished and more broadened than those of the graphene electrodes; that is, the observed oscillations appear dampened when compared to the graphene cases. This dampening is a result of a combination of two factors. According to Gauss's law, the electric field strength decays radially in the CNT case ($E = \sigma R/\varepsilon_0 r$)[44] while remaining constant in the graphene case ($E = \sigma/\varepsilon_0$); the weaker electrostatic attraction between the electrode and the electrolyte leads to a more diffuse behavior. In addition, the space available (*i.e.* volume) for IL ions to populate (relative to the electrode surface area) is larger and increases radially in the CNT case, which also serves to broaden the mass density peaks. The peak (average) density of PF_6 in the first layer near the positively charged CNT is 1.85 (1.04) g cm^{-3}, which is smaller than 2.23 (1.27) g cm^{-3} in the first layer near positively charged graphene. Similarly near the negative CNT electrode, the peak (average) density of BMIM in the first layer is 2.39 (1.01) g cm^{-3}, which is also smaller than 3.29 (1.10) g cm^{-3} in the graphene case. This suggests that the counterions near the CNT cannot fill the space at the interface as efficiently as the graphene case; that is, the ions are packed less densely near curved surfaces. Here we should note that despite the lower packing density, the absolute number of counterions relative to the electrode surface area is larger in the CNT case (not shown) due to the larger relative volume of space surrounding the electrode and is in good agreement with previous simulations.[26]

For each system, the space charge density (ρ_q) in the IL electrolyte was calculated based on the distribution of IL atoms with fixed atomic charges and shown in Fig. 3. Near both the neutral and positive electrodes, the charge density peaks in the CNT case [Fig. 3(a) and (b)] are reduced and broadened when compared to the graphene case [Fig. 3(d) and (e)]; this follows directly from the reduced packing density as indicated from the mass density profiles [Fig. 2]. Near the negative electrodes, however, the charge density peaks in the CNT case [Fig. 3(c)] exhibit larger fluctuations compared to the graphene case [Fig. 3(f)]. While the profile of the first peak (which is attributed to BMIM) is nearly the same for both electrode types, the valley (which is attributed to PF_6) is more distinct in the CNT case. This suggests that PF_6 co-ions in the CNT case have a greater tendency to mix with the BMIM counterions in the first layer, which will influence the electric potential profiles as discussed later.

From ρ_q, the electric potential (ϕ) profiles along the electrode surface normal direction were calculated by solving Poisson's equation and are given by

$$\phi(z) = \begin{cases} -\dfrac{\sigma R}{\varepsilon_0}\ln\dfrac{r}{R} - \dfrac{1}{\varepsilon_0}\int_R^r \rho_q(r')r'\ln\dfrac{r}{r'}\mathrm{d}r' & \text{CNT} \\ -\dfrac{\sigma z}{\varepsilon_0} - \dfrac{1}{\varepsilon_0}\int_0^z (z-z')\rho_q(z')\mathrm{d}z' & \text{Graphene} \end{cases} \quad (1)$$

where z is the distance from the graphene electrode.

The calculated ϕ profiles for both the CNT and graphene cases are shown in Fig. 4. When $\sigma = 0$ μC cm^{-2}, the PZC, which was determined by the difference between the IL bulk potential and the electrode surface potential [Fig. 4(a)] is nearly zero for both the graphene and CNT cases (20 and −40 meV, respectively), in good agreement with previous simulation results.[26,45] From Fig. 4(b) and (c), it is evident that the potential drops more rapidly at the graphene interface, deviating by 0.5 V more than that of the CNT system at 2.5 Å from the surface. This is a result of the aforementioned decay in the electric field strength

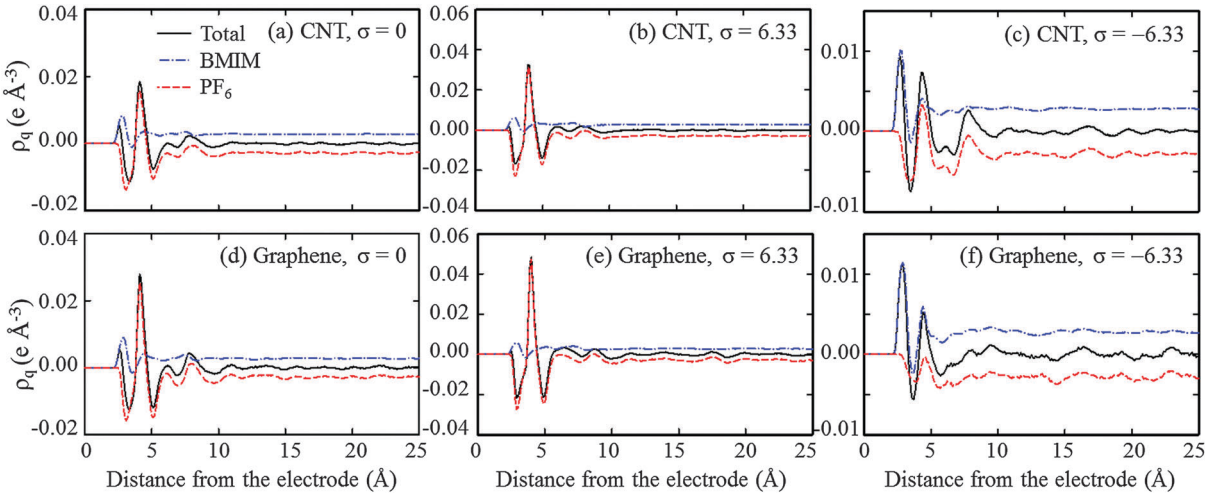

Fig. 3 Total BMIM and PF_6 space charge density (ρ_q) profiles near (6,6) CNT [(a)–(c)] and pristine graphene [(d)–(f)] electrodes at the listed σ (in μC cm^{-2}) as a function of distance from the electrode surface.

near the CNT electrode. Near the positive electrode [Fig. 4(b), σ = +6.33 μC cm^{-2}], ϕ_D (the bulk potential – electrode surface potential) is predicted to be 1.40 and 1.14 V for the graphene and CNT cases, respectively, suggesting that the smaller potential drop near the CNT is primarily due to the initial potential drop, which in turn is attributed to geometric factors. Near the negative electrode [Fig. 4(c), σ = −6.33 μC cm^{-2}], ϕ_D for the graphene and CNT cases are −1.18 and −1.07 V, respectively. Unlike the positive side, the difference in ϕ_D which stems from geometric factors seems to be mitigated by the IL charge distribution. Recall that near the negative electrode, PF_6 co-ions have a greater tendency to mix with BMIM counterions near the CNT electrodes. As a result, the ability of the IL ions to screen the electric field is effectively lowered. This is especially apparent in Fig. 4(c) around 3–4 Å away from the CNT electrode where the first layer of IL ions is located. As shown in the graphene case, if the first layer is highly rich in counterions, we can expect ϕ to monotonically decrease. The CNT case, however, shows a small hump (or increase) in ϕ, ensuing a net increase of $|\phi_D|$ that is closer to the graphene case.

Table 1 Potential drop in the EDL (ϕ_D) and double layer capacitance (C_D) at the listed σ for the graphene/CNT cases

σ (μC cm^{-2})	0.40	−0.40	6.33	−6.33
ϕ_D (V)[a]	0.13/0.041	−0.044/−0.089	1.40/1.14	−1.18/−1.07
C_D (μF cm^{-2})	3.57/4.78	6.19/8.38	4.59/5.36	5.26/6.16

[a] The predicted PZC of the graphene–IL and CNT–IL systems is 0.02 V and −0.04 V, respectively.

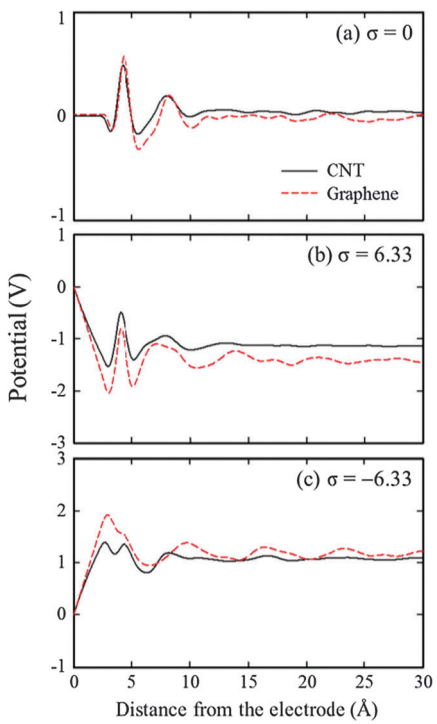

Fig. 4 Comparison of potential profiles between the CNT and graphene cases with respect to the surface potential at the listed σ (in μC cm^{-2}) as a function of distance from the electrode surface.

In Table 1, we present the predicted C_D at σ = 0, ±0.40, and ±6.33 μC cm^{-2} for both electrode cases. At each σ, the predicted C_D for the CNT case ($C_{D,CNT}$) tends to be greater than that of graphene ($C_{D,Gr}$). Furthermore, the impact of curvature on C_D seems to be larger at lower σ; the C_D at σ = ±0.40 μC cm^{-2} is enhanced by around 35% while at σ = ±6.33 μC cm^{-2}, the enhancement is around 17%. As discussed previously, the decay of the electric field strength near the CNT lends itself to a smaller ϕ_D and therefore, C_D enhancement.

3.2. Electronic structure and quantum capacitance

For low-dimensional materials, it is known that the capacitance is quantized; Luryi first formalized the concept of the quantum capacitance for graphene which was treated as a two-dimensional electron gas.[46] In the case of one-dimensional (1D) CNTs, the quantum capacitance is defined as $C_Q = d\sigma/d\phi_C$, where $d\sigma$ and $d\phi_C$ refer to variations of charge density and local potential of

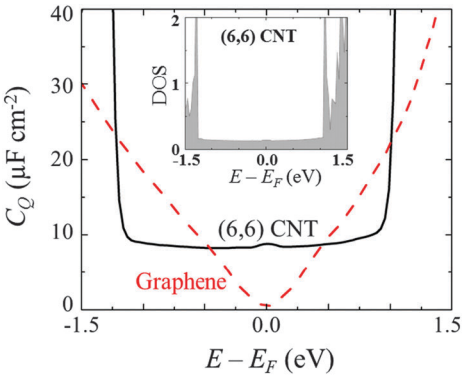

Fig. 5 Comparison of quantum capacitance (C_Q) between the (6,6) CNT and graphene electrodes. E_F indicates the Fermi level. The inset shows the DOS (in eV^{-1} Å^{-1}) of the CNT.

the CNT. Provided that the electrochemical potential μ of the electrode is rigidly shifted by $e\phi_C$, C_Q can be given by[29]

$$C_Q = e^2 \int_{-\infty}^{+\infty} D(E) F_T(E - \mu) dE \quad (2)$$

where e is the elementary charge, $D(E)$ is the 1D electron density of states (DOS), E is the relative energy with respect to E_F, and F_T [$= (4kT)^{-1}\mathrm{sech}^2(E/2kT)$] is the thermal broadening function. Here, we do not consider any shifts in E_F which may occur due to charge transfer between [BMIM][PF$_6$] and the electrodes, as also previously reported.[47]

The DOS of a (6,6) CNT was estimated using DFT calculations, as shown in the inset of Fig. 5. One important feature to note is that the DOS is nearly constant ($\approx$0.15 eV^{-1} Å^{-1}) when $|E| < 1.0$ eV, before dramatically increasing at the so-called Van Hove singularity. The DOS of metallic CNTs near the Fermi level can also be approximated with the nearest-neighbor tight-binding (NNTB) formalism[48]

$$D(E) = \frac{8}{3a\pi\gamma} \quad \text{for} |E| < |E_{vh}| \quad (3)$$

where γ ($\approx$2.5 eV) is the nearest neighbor interaction parameter, a is the C–C bond length, and E_{vh} is the energy of the first Van Hove singularity. The approximated DOS in this energy range ($\approx$0.14 eV^{-1} Å^{-1}) shows good agreement with the DFT calculations [inset in Fig. 5].

Using eqn (2) and the DOS (calculated with DFT), we estimated the C_Q of the CNT ($C_{Q,CNT}$), as shown in Fig. 5. The $C_{Q,CNT}$ exhibits a constant profile with a value around 9.0 μF cm^{-2} when $|\phi_C| < 1.0$ V. When $|\phi_C| < 0.5$ V, it is clear that $C_{Q,CNT}$ is larger compared to the C_Q of pristine graphene ($C_{Q,Gr}$) [dashed line in Fig. 5], which is apparently due to the greater abundance of states in the CNT case near the Fermi level. However, the $C_{Q,Gr}$ is estimated to be larger than $C_{Q,CNT}$ when $0.5 < |\phi_C| < 1.0$ V, before $C_{Q,CNT}$ becomes larger once again.

3.3. The total interfacial capacitance

The total interfacial capacitance (C_T) can be modeled as a series of C_Q and C_D, *i.e.*, $1/C_T = 1/C_Q + 1/C_D$. With the calculated values of C_Q and C_D, we estimated C_T as a function of applied

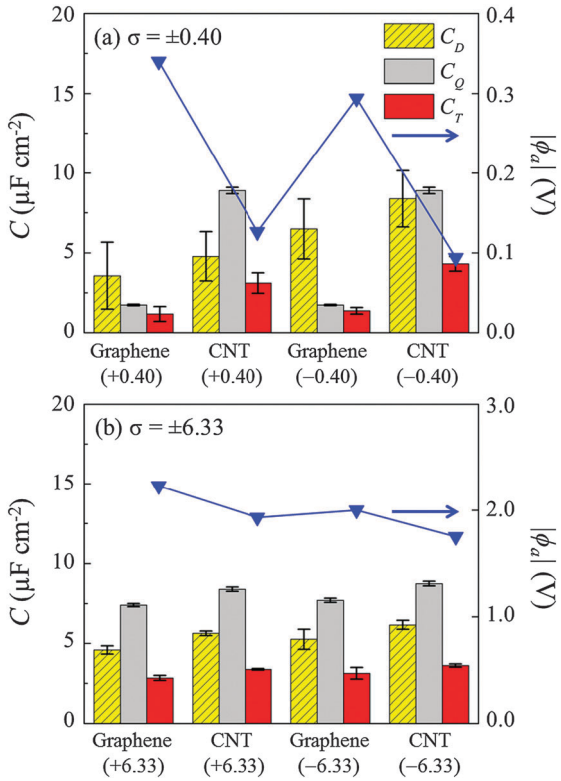

Fig. 6 The double layer (C_D), quantum (C_Q), and total interfacial (C_T) capacitance at the listed σ (in μC cm^{-2}). The (▼) indicates the corresponding applied potential (ϕ_a).

potential ϕ_a ($\phi_a = \phi_D + \phi_C$), as shown in Fig. 6. Here, the relationship between C_Q and C_D with ϕ_a was obtained through σ; recall that $C_Q/C_D \propto \sigma \propto \phi_C/\phi_D$.[29] Note that in this case, we use the integral $C_Q = \sigma/\phi_C$. When $\sigma = \pm 0.40$ μC cm^{-2} [Fig. 6(a)], the C_T for the CNT electrode is predicted to be $C_{T,CNT} \approx 3.1$–4.3 μF cm^{-2} which is 2.6–3.1 times larger than the graphene case with $C_{T,Gr} \approx 1.2$–1.4 μF cm^{-2}. According to our calculations, the capacitance enhancement in the CNT case can be attributed to the larger values in both $C_{Q,CNT}$ and $C_{D,CNT}$ compared to those in the graphene case. However, when $\sigma = \pm 6.33$ μC cm^{-2} [Fig. 6(b)], $C_{T,Gr}$ and $C_{T,CNT}$ are much more comparable ($\approx$2.8–3.6 μF cm^{-2}) although $C_{T,CNT}$ is around 15–20% larger than $C_{T,Gr}$. This is primarily due to the large increase (decrease) in $C_{Q,Gr}$ ($C_{Q,CNT}$) such that both $C_{Q,CNT}$ and $C_{D,CNT}$ are around 14–22% larger than the respective graphene cases. Based on our results, we suspect that at low σ/ϕ_a, the CNT electrode may perform significantly better than the graphene electrode due to the combination of higher $C_{D,CNT}$ and lower $C_{Q,Gr}$. At higher σ/ϕ_a, however, the shifting relative contributions of C_Q and C_D could diminish the benefit of the CNT electrodes.

Kim and coworkers recently demonstrated that using CNTs grown on graphene could outperform the C_T of graphene-only electrodes.[49] While this enhancement may partially be due to the influence of electrode curvature on C_D and C_Q, we must recognize that other issues, such as increased electrolyte accessibility, can also be important. Here, we should note that additional factors

may need to be considered for more quantitative analysis of the C_T. For instance, we have neglected the possible polarization of the electrodes[50] and IL ions at the interface and its effect on the electrode charge redistribution, the space charge density, and subsequently, C_D. In addition, the DOS (and C_Q) may be altered to a certain extent if the electronic structure is locally modified by electrode–IL interactions, which were omitted for simplicity. Nonetheless, our work clearly highlights the importance of both C_Q and C_D in understanding the performance of CNT-based supercapacitors.

Finally, this study raises several questions for future research. For instance, the C_Q and C_D of CNTs could depend upon their chirality and diameter. For semiconducting CNTs, for example, C_Q will be zero near the Fermi level and the bandgap will vary inversely with the CNT diameter.[51] Beyond CNTs, other carbon nanostructures have been explored as potential electrode candidates. However, it would be important to recognize that the structural differences of these electrodes can have a profound impact on not only C_D, but also C_Q. The future design of nanostructured carbon-based electrodes with various topologies, then, would greatly benefit from an in-depth study on the specific impact of structural modification on C_Q as compared to C_D.

4. Conclusions

We theoretically evaluated the interfacial capacitance of (6,6) CNT electrodes in [BMIM][PF_6] IL and compared the performance to graphene electrodes, with particular attention to the relative contributions of the electrode quantum (C_Q) and EDL capacitance (C_D). Our MD simulations reveal that the CNT electrodes improve the C_D ($\approx\sigma/\phi_D$) when compared to the graphene electrodes by around 35% when $\sigma = \pm 0.40$ μC cm^{-2}, which reduces to around 17% when $\sigma = \pm 6.33$ μC cm^{-2}. Our analysis suggests that the lower EDL potential drop (ϕ_D) with the CNT is largely attributed to the reduced electric field strength at the CNT–IL interface. Such geometric effect tends to be mitigated as a result of poor segregation of cations and anions near the curved surface; this is especially apparent near the negative electrode where BMIM cations unsuccessfully obstruct PF_6 anions. According to our DFT calculations, the C_Q of the (6,6) CNT is nearly constant (9 μF cm^{-2}) and significantly larger than graphene near the Fermi level, which is apparently a result of the increased availability of electron states. At low applied voltage ($\phi_a < 0.5$ V), the total interfacial capacitance (C_T) of the CNT case is predicted to be about three times that of the graphene case, due to both a larger C_Q and C_D. However, the enhancement of C_T is likely diminished (predicted to be 15–20% increase) at higher ϕ_a (≈ 2 V) due to the increase (decrease) in $C_{Q,Gr}$ ($C_{Q,CNT}$); this clearly demonstrates that the curvature effect is a strong function of ϕ_a. Our study highlights that the capacitive performance of carbon-based nanomaterials can be substantially improved by tailoring their topologies, while the structural modifications tend to have a profound impact on both C_Q and C_D and warrant further study.

Acknowledgements

This work was partially supported by the R.A. Welch foundation (F-1535) and the U.S. Department of Energy, Office of Basic Energy Sciences, Division of Materials Sciences and Engineering (DE-SC001951). We would like to thank the Texas Advanced Computing Center for use of their computing resources. Helpful discussion with Rodney S. Ruoff is also greatly acknowledged.

Notes and references

1 G. Wang, L. Zhang and J. Zhang, *Chem. Soc. Rev.*, 2012, **41**, 797–828.
2 B. E. Conway, *Electrochemical Supercapacitors: Scientific Fundamentals and Technological Applications*, New York, Kluwer Academic, 1999.
3 R. D. Rogers and K. R. Seddon, *Science*, 2003, **302**, 792.
4 W. Xu and C. A. Angell, *Science*, 2003, **302**, 422.
5 A. Lewandowski and M. Galinski, *J. Phys. Chem. Solids*, 2004, **65**, 281.
6 P. Simon and Y. Gogotsi, *Nat. Mater.*, 2008, **7**, 84.
7 H. Jiang, P. Lee and C. Li, *Energy Environ. Sci.*, 2012, **6**, 41.
8 Y. Wang, Z. Shi, Y. Huang, Y. Ma, C. Wang, M. Chen and Y. Chen, *J. Phys. Chem. C*, 2009, **113**, 13103–13107.
9 X. Huang, X. Qi, F. Boey and H. Zhang, *Chem. Soc. Rev.*, 2012, **41**, 666–686.
10 B. B. Garcia, S. L. Candelaria and G. Cao, *J. Mater. Sci.*, 2012, **47**, 5996–6004.
11 H. Guo and Q. Gao, *J. Power Sources*, 2009, **186**, 551–556.
12 A. K. Mishra and S. Ramaprabhu, *J. Phys. Chem. C*, 2011, **115**, 14006–14013.
13 Z. J. Li, T. X. Chang, G. Q. Yun and Y. Jia, *Powder Technol.*, 2012, **224**, 306–310.
14 H. M. Jeong, J. W. Lee, W. H. Shin, Y. J. Choi, H. J. Shin, J. K. Kang and J. W. Choi, *Nano Lett.*, 2011, **11**, 2472–2477.
15 B. Jiang, C. Tian, L. Wang, L. Sun, C. Chen, X. Nong, Y. Qiao and H. Fu, *Appl. Surf. Sci.*, 2012, **258**, 3438–3443.
16 Y. Qiu, X. Zhang and S. Yang, *Phys. Chem. Chem. Phys.*, 2011, **13**, 12554–12558.
17 L. Sun, L. Wang, C. Tian, T. Tan, Y. Xie, K. Shi, M. Li and H. Fu, *RSC Adv.*, 2012, **2**, 4498.
18 K. H. An, W. S. Kim, Y. S. Park, Y. C. Choi, S. M. Lee, D. C. Chung, D. J. Bae, S. C. Lim and Y. H. Lee, *Adv. Mater.*, 2001, **13**, 497–500.
19 D. N. Futaba, K. Hata, T. Yamada, T. Hiraoka, Y. Hayamizu, Y. Kakudate, O. Tanaike, H. Hatori, M. Yumura and S. Iijima, *Nat. Mater.*, 2006, **5**, 987–994.
20 Y. Honda, T. Haramoto, M. Takeshiga, H. Shiozaki, T. Kitamura, K. Yoshikawa and M. Ishikawa, *J. Electrochem. Soc.*, 2008, **155**, A930.
21 M. Kaempgen, C. K. Chan, J. Ma, Y. Cui and G. Gruner, *Nano Lett.*, 2009, **9**, 1872–1876.
22 W. Lu, L. Qu, K. Henry and L. Dai, *J. Power Sources*, 2009, **189**, 1270–1277.
23 B. W. Kim, H. G. Chung, B. K. Min, H. G. Kim and W. Kim, *Bull. Korean Chem. Soc.*, 2010, **31**, 3697–3702.

24 L. Yang, B. H. Fishbine, A. Migliori and L. R. Pratt, *J. Am. Chem. Soc.*, 2009, **131**, 12373–12376.
25 J. Huang, B. G. Sumpter, V. Meunier, G. Yushin, C. Portet and Y. Gogotsi, *J. Mater. Res.*, 2010, **25**, 1525.
26 G. Feng, R. Qiao, J. Huang, S. Dai, B. G. Sumpter and V. Meunier, *Phys. Chem. Chem. Phys.*, 2011, **13**, 1152.
27 J. Xia, F. Chen, J. Li and N. Tao, *Nat. Nanotechnol.*, 2009, **4**, 505.
28 M. D. Stoller, C. W. Magnuson, Y. Zhu, S. Murali, J. W. Suk, R. Piner and R. S. Ruoff, *Energy Environ. Sci.*, 2011, **4**, 4685.
29 E. Paek, A. J. Pak and G. S. Hwang, *J. Electrochem. Soc.*, 2013, **160**, A1–A10.
30 E. Paek, A. J. Pak, K. E. Kweon and G. S. Hwang, *J. Phys. Chem. C*, 2013, **117**, 5610–5616.
31 W. L. Jorgensen, D. S. Maxwell and J. Tirado-Rives, *J. Am. Chem. Soc.*, 1996, **118**, 11225.
32 G. Kaminski and W. L. Jorgensen, *J. Phys. Chem.*, 1996, **100**, 18010.
33 W. Hoover, *Phys. Rev. A*, 1985, **31**, 1695.
34 S. J. Plimpton, *J. Comput. Phys.*, 1995, **117**, 1.
35 J. P. Perdew and Y. Wang, *Phys. Rev. B: Condens. Matter Mater. Phys.*, 1992, **45**, 13244.
36 G. Kresse and J. Furthmüller, *Phys. Rev. B: Condens. Matter Mater. Phys.*, 1996, **54**, 11169.
37 P. E. Blöchl, *Phys. Rev. B: Condens. Matter Mater. Phys.*, 1994, **50**, 17953.
38 H. J. Monkhorst and J. D. Pack, *Phys. Rev. B: Solid State*, 1976, **13**, 5188.
39 S. Wang, S. Li, Z. Cao and T. Yan, *J. Phys. Chem. C*, 2010, **114**, 990.
40 S. Maolin, Z. Fuchun, W. Guozhong, F. Haiping, W. Chunlei, C. Shimou, Z. Yi and H. Jun, *J. Chem. Phys.*, 2008, **128**, 134504.
41 S. A. Kislenko, I. S. Samoylov and R. H. Amirov, *Phys. Chem. Chem. Phys.*, 2009, **11**, 5584.
42 M. Mezger, H. Schroder, H. Reichert, S. Schramm, J. S. Okasinski, S. Schroder, V. Honkimaki, M. Deutsch, E. M. Ocko, J. Ralston, M. Rohwerder and M. Stratmann, *Science*, 2008, **322**, 424.
43 S. Bovio, A. Podesta, C. Lenardi and P. Milani, *J. Phys. Chem. B*, 2009, **113**, 6600.
44 R is the CNT radius, ε_0 is the vacuum permittivity, and r is the distance from the CNT center.
45 S. Wang, S. Li, Z. Cao and T. Yan, *J. Phys. Chem. C*, 2010, **114**, 990.
46 S. Luryi, *Appl. Phys. Lett.*, 1988, **52**, 501.
47 M. H. Ghatee and F. Moosavi, *J. Phys. Chem. C*, 2011, **115**, 5626–5636.
48 R. Saito, M. S. Dresselhaus and G. Dresselhaus, *Physical Properties of Carbon Nanotubes*, Imperial College Press, 1998.
49 Y.-S. Kim, K. Kumar, F. T. Fisher and E.-H. Yang, *Nanotechnology*, 2012, **23**, 015301.
50 C. Merlet, C. Péan, B. Rotenberg, P. A. Madden, P. Simon and M. Salanne, *J. Phys. Chem. Lett.*, 2013, **4**, 264.
51 C. White and J. Mintmire, *J. Phys. Chem. B*, 2005, **109**, 52–65.